Neuroscience Letters 553 (2013) 84–89

Contents lists available at ScienceDirect

Neuroscience Letters

journal homepage: www.elsevier.com/locate/neulet

Classification of functional near-infrared spectroscopy signals corresponding to the right- and left-wrist motor imagery for development of a brain–computer interface

Noman Naseer [a], Keum-Shik Hong [a,b,*]

[a] Department of Cogno-Mechatronics Engineering, Pusan National University, 30 Jangjeon-dong, Geumjeong-gu, Busan 609-735, Republic of Korea
[b] School of Mechanical Engineering, Pusan National University, 30 Jangjeon-dong, Geumjeong-gu, Busan 609-735, Republic of Korea

HIGHLIGHTS

- Classification of fNIRS signals corresponding to the right- and left-wrist motor imagery.
- Hemodynamic responses of the right-wrist imagery are distinguishable from those of left.
- Signal slope improves the classification accuracy significantly than signal mean.
- Enhanced performance on examination of subset of the response data.

ARTICLE INFO

Article history:
Received 14 May 2013
Received in revised form 5 August 2013
Accepted 12 August 2013

Keywords:
Functional near-infrared spectroscopy (fNIRS)
Brain–computer interface (BCI)
Wrist motor imagery

ABSTRACT

This paper presents a study on functional near-infrared spectroscopy (fNIRS) indicating that the hemodynamic responses of the right- and left-wrist motor imageries have distinct patterns that can be classified using a linear classifier for the purpose of developing a brain–computer interface (BCI). Ten healthy participants were instructed to imagine kinesthetically the right- or left-wrist flexion indicated on a computer screen. Signals from the right and left primary motor cortices were acquired simultaneously using a multi-channel continuous-wave fNIRS system. Using two distinct features (the mean and the slope of change in the oxygenated hemoglobin concentration), the linear discriminant analysis classifier was used to classify the right- and left-wrist motor imageries resulting in average classification accuracies of 73.35% and 83.0%, respectively, during the 10 s task period. Moreover, when the analysis time was confined to the 2–7 s span within the overall 10 s task period, the average classification accuracies were improved to 77.56% and 87.28%, respectively. These results demonstrate the feasibility of an fNIRS-based BCI and the enhanced performance of the classifier by removing the initial 2 s span and/or the time span after the peak value.

1. Introduction

A brain–computer interface (BCI) provides a means of controlling machines and robots for locked-in people by interpreting the neuronal signals from the brain directly and bypassing the signals from the peripheral nerves and muscles [34]. Recently, researchers successfully trained people with head-implanted microelectrodes to control robotic and prosthetic arms [10]. Noninvasive methods, however, are preferable to avoid the inherent medical risks in microelectrode implantation. Various noninvasive modalities including electroencephalography (EEG), magnetoencephalography (MEG), functional magnetic resonance imaging (fMRI), and functional near-infrared spectroscopy (fNIRS) are currently being used to acquire brain signals for BCI applications.

fNIRS is a novel brain imaging technology that is used to measure the hemodynamic response of the cerebral cortex using near-infrared (NI) light (650–1000 nm) [11,35]. The fNIRS technique is based on the measurement of hemodynamic changes in the cerebral blood flow, that is, the concentration changes of oxygenated hemoglobin (HbO) and deoxygenated hemoglobin (HbR). fNIRS employs multiple emitter/detector pairs of NI lights operating at two or more different wavelengths. The lights emitted into the scalp diffuse through the brain tissues due to multiple scattering of photons. While the majority of the lights are absorbed in the tissues or continue to scatter, a portion of lights exit the scalp after passing through the cortical area, wherein the HbO and HbR chromophores in the path absorb them with different absorption coefficients. The

* Corresponding author at: Department of Cogno-Mechatronics Engineering, Pusan National University,30 Jangjeon-dong, Geumjeong-gu, Busan 609-735, Republic of Korea. Tel.: +82 51 510 2454; fax: +82 51 514 0685.
E-mail addresses: noman@pusan.ac.kr (N. Naseer), kshong@pusan.ac.kr (K.-S. Hong).

0304-3940/$ – see front matter © 2013 Elsevier Ireland Ltd. All rights reserved.
http://dx.doi.org/10.1016/j.neulet.2013.08.021

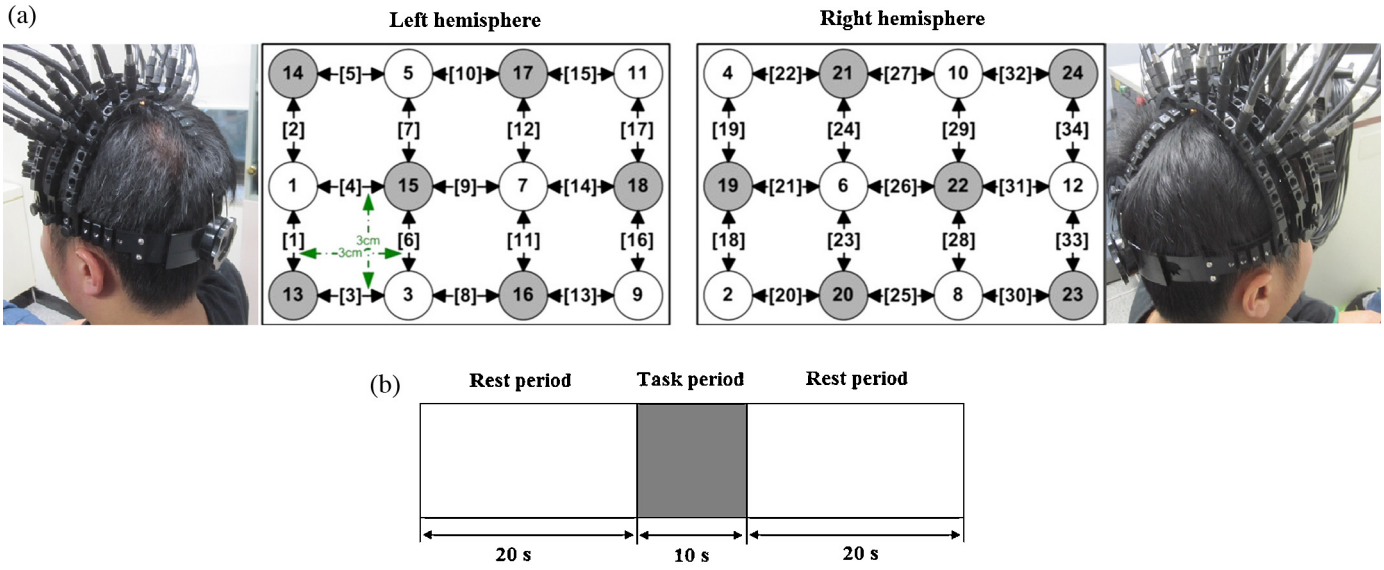

Fig. 1. (a) Optode placement and channel configuration: Each gray-filled circle represents an emitter, and each unfilled circle represents a detector. (b) Schematic illustration of the experimental paradigm used: The white blocks represent the 20 s rest periods at the beginning and at the end; the gray-filled block represents the 10 s task period.

exited photons are detected using strategically positioned detectors, and the intensity of the detected light is then used to calculate the HbO and HbR concentration changes (ΔHbO and ΔHbR) along the photon path. The principle of fNIRS measurement, first reported by Jobsis [16], has been applied to the study of cerebral hemodynamics for more than two decades, even though its use in brain mapping, brain-state decoding, and BCI is only a few years old [1,2,5,6,12–15,17,21,26,27,30,31]. The major advantages of fNIRS are its noninvasiveness, relatively low cost, portability, and wearability. Since fNIRS is an optical modality, its measurements are not susceptible to electrogenic artifacts [20].

In the present research, the adopted brain signal generation paradigm is motor imagery. Motor imagery can be defined as the mental rehearsal of motor acts that is not accompanied by overt body movements. It is a mental task often employed for BCI applications, and has been shown to work well in previous EEG-based BCI studies [23,24,29,33]. Indeed, Beisteiner et al. [3] demonstrated that the brain activation during a motor imagery is similar to the brain activation during the associated motor execution (overt body movement). Motor imagery tasks should be easy to learn and execute and, moreover, the use-friendliness of the BCI system is important. Motor imagery signal decoding, besides its significance to BCI development, is appealing from the prospective of neurorehabilitation.

In this study, by classifying the right- and left-wrist motor imagery signals, we achieved a significant advance towards an fNIRS-based BCI. After acquiring the fNIRS signals representing the right- and left-wrist motor imageries from the primary motor cortex, those signals were normalized and filtered. By using two distinct features (the mean and the slope of the signal), they were classified into two classes, “right-wrist motor imagery” and “left-wrist motor imagery.” The average classification accuracy was as high as 87.28%. The contributions of this study are as follows: (i) To the best of the authors’ knowledge, this is the first work on the classification of fNIRS signals corresponding to the right- and left-wrist motor imageries; (ii) it has been illustrated that the signal slope (SS), as a classification feature, offers significantly better classification accuracy than the signal mean (SM); (iii) it is found that the classifier performance can be enhanced when the analysis is performed on the focused time period, for instance, during 2–7 s time interval instead of the overall 10 s task period.

2. Experimental procedure

2.1. Participants

A total of 10 healthy adults were recruited (all male, right handed, mean age: 28.5 ± 4.8). Only right handed participants were sought, so as to minimize any variations in the hemodynamic responses due to the hemispheric-dominance difference. None of the participants had a history of any psychiatric, neurological or visual disorder. All of them had normal or corrected-to-normal vision, and all provided a verbal consent after they were informed in detail about the experimental procedure. The experiment was conducted in accordance with the latest Declaration of Helsinki.

2.2. Optode placement and channel configuration

Since motor imagery activates the brain’s primary motor cortex [3,25], a total of 12 NI light emitters and 12 detectors were positioned over the left and right hemispheres to measure the signals from the left and right primary motor cortices. With the optodes configuration in Fig. 1(a), 17 interconnecting channels were made on each hemisphere by considering the imaging depth related to the emitter–detector distance [7–9,19,22]. For measurement of signals from the cortical area, an approximately 30 mm emitter–detector distance has been set [7]. Channels covering an emitter–detector distance of more than 30 mm were discarded, as it is not certain whether the signals received at such channels were through the cortical area or not and in any case the signal might be too weak to be used [9].

2.3. Experimental protocol

Each participant was seated in a comfortable chair facing a 15.6 in. monitor situated at a distance of 65–70 cm in a dimly lighted room. He was asked to relax for at least 5 min prior to the experiment in order to settle his heart rate and blood pressure down and to remain relaxed through the experiment so as to avoid, to the extent possible, any unnecessary movement or thinking. In each trial during the experiment, the first 20 s was a rest period to set up the baseline, followed by a 10 s task period, which was followed in turn by another 20 s rest period, for a total trial duration of 50 s.

Table 1
The classification accuracies with standard deviations according to the two features (SM and SS) for data acquired in the two time windows (20–30 s, 22–27 s).

Participant number	SM 20–30 [%]	SS 20–30 [%]	SM 22–27 [%]	SS 22–27 [%]
1	75.3 ± 8.24	84.2 ± 6.81	78.9 ± 5.49	87.7 ± 6.53
2	77.8 ± 6.17	89.5 ± 7.64	81.6 ± 6.71	93.2 ± 5.74
3	68.3 ± 7.43	78.8 ± 6.14	75.3 ± 4.67	84.6 ± 7.19
4	72.3 ± 5.91	82.1 ± 5.27	73.9 ± 6.54	83.7 ± 6.27
5	75.5 ± 9.43	84.9 ± 7.25	70.3 ± 5.76	89.5 ± 6.98
6	70.1 ± 8.10	79.9 ± 5.94	75.4 ± 8.85	86.2 ± 5.49
7	74.5 ± 6.44	83.5 ± 8.46	82.2 ± 6.94	85.8 ± 6.37
8	69.9 ± 9.57	78.9 ± 7.55	78.7 ± 6.81	90.1 ± 5.20
9	72.8 ± 5.33	81.6 ± 6.94	80.4 ± 5.46	88.2 ± 8.26
10	77.0 ± 6.43	86.6 ± 5.83	78.9 ± 7.73	83.8 ± 7.86
Average	73.35 ± 3.20	83.0 ± 3.45	77.56 ± 3.75	87.28 ± 3.06

This experimental paradigm is shown in Fig. 1(b). During the task period, each participant was asked to imagine moving his left or right wrist upwards (flexion), which movement was indicated on the monitor in a pseudorandom way. The imagined movement was self-paced at around 4–5 movements during the task period. All of the participants took part in a training session preparatory to the actual experiments.

2.4. Signal acquisition and signal processing

A multichannel continuous-wave imaging system (DYNOT: DYnamic Near-infrared Optical Tomography; two wavelengths: 760 and 830 nm) obtained from NIRx Medical Technologies, NY, was used to acquire brain signals at a sampling rate of 1.81 Hz. The raw signals were first normalized by dividing them by the mean value of the baseline signal during the rest period. In order to minimize the physiological noise due to heart pulsation (1–1.5 Hz for adults), respiration (approximately 0.4 Hz for adults), and blood pressure (Mayer) waves (approximately 0.1 Hz), the signals were then low-pass filtered using a 4th order Butterworth filter at a cut-off frequency of 0.1 Hz. The relative concentration changes ΔHbX (i.e., ΔHbO and ΔHbR) were then calculated, with reference to the dual-wavelength light intensity signals and the modified Beer-Lambert law, as follows.

$$\begin{bmatrix} \Delta\phi_{\mathrm{HbO}}(t) \\ \Delta\phi_{\mathrm{HbR}}(t) \end{bmatrix} = \begin{bmatrix} a_{\mathrm{HbO}}(\lambda_1) & a_{\mathrm{HbR}}(\lambda_1) \\ a_{\mathrm{HbO}}(\lambda_2) & a_{\mathrm{HbR}}(\lambda_2) \end{bmatrix}^{-1} \begin{bmatrix} \Delta\phi(t;\lambda_1) \\ \Delta\phi(t;\lambda_2) \end{bmatrix}, \quad (1)$$

$$\Delta\mathrm{HbX}(t) = \frac{\Delta\phi_{\mathrm{HbX}}(t)}{d \times l}, \quad (2)$$

where $\Delta\phi_{\mathrm{HbX}}(t)$ is the optical density variation of HbX in μM mm, $\Delta\phi(\mathrm{t};\ \lambda_j)$ ($j = 1, 2$) is the unit-less total optical density variation of the light emitter of wavelength λ_j, $a_{\mathrm{HbX}}(\lambda_j)$ is the extinction coefficient of HbX in $\mu\mathrm{M}^{-1}\,\mathrm{mm}^{-1}$, d is the unit-less differential pathlength factor, and l is the distance (in millimeters) between emitter and detector.

2.5. Classification

The classification methodology employed in the present study was linear discriminant analysis (LDA), and only ΔHbO signals were considered for classification. LDA, a linear classifier, uses hyper-planes to discriminate between the different classes of data [18]. The separating hyper-plane is designed to maximize the distance between the class means and minimize the interclass variances. Owing to its simplicity and execution speed, LDA performed well in a number of BCI problems [18,27–29]. The classifier features considered were SM and SS, since the hemodynamic response typically appears as an increase in ΔHbO and a decrease in ΔHbR [4]. These two features have been shown to work well in the previous studies [6,20,21,26]. Classification was performed on the signals acquired during the smaller 2–7 s time span within the task period (i.e., for 22–27 s span if the rest period is included) as well as the whole 10 s task period (i.e., for 20–30 s span if the rest period is included). The reason for selecting the former is that the hemodynamic response lags the neuronal event by approximately 2 s and takes approximately 5 s to reach its peak value. The SS value from 20 to 30 s (i.e., SS 20–30) and that from 22 to 27 s (i.e., SS 22–27) were determined by fitting a line to all of the data points in the 20–30 s and 22–27 s time windows, respectively, using linear regression, while the SM value from 20 to 30 s (i.e., SM 20 to 30) and that from 22 to 27 s (i.e., SM 22–27) were determined by averaging all the data points in the respective time windows. Since nonscaled data usually tend to over-fitting [32], scaling was performed prior to classification. The classification accuracies were estimated using ten runs of a five-fold cross-validation.

3. Results

Table 1 lists the participants' classification accuracies that were averaged over all the channels and all the trials for each participant. The average accuracy using SM 20–30 was found to be 73.35%, whereas that using SS 20–30 was 83.0%. Also, by using the 22–27 s time window (i.e., SM 22–27 and SS 22–27), both accuracies were improved resulting in 77.56% and 87.28%, respectively. The best accuracy out of 4 cases was 87.28%, which was achieved by SS 22–27.

Comparing the results in two time windows, the p-value for SM 22–27 versus SM 20–30 was 0.0146, whereas that for SS 22–27 versus SS 20–30 was 0.0089, indicating that both features performed significantly better in the 22–27 s time window. The p-value for SS 20–30 versus SM 20–30 and that for SS 22–27 versus SM 22–27 were 4.27×10^{-6} and 5.58×10^{-6}, respectively, which show that in both time windows, SS performed significantly better as a feature than did SM. Fig. 2 shows the ΔHbO responses for the first four participants for both the right- and left-wrist motor imagery. Fig. 3 shows the grand averages of ΔHbO across all of the participants for the right- and left-wrist motor imageries.

4. Discussions

The average classification accuracies achieved from the right- and left-wrist motor imageries were very encouraging. In fact, they were greatly enhanced when classification was performed on the signals acquired during the 22-27 s period. To verify the best performance of the classifier during that period, classifications on signals acquired during 22–28 s, 22–29 s, 22–30 s, and 25–30 s windows were also performed. The classification accuracies achieved using SS during those time windows (SS 22–28, SS 22–29, SS 22–30 and SS 25–30) are listed in Table 2. Although the classification accuracies

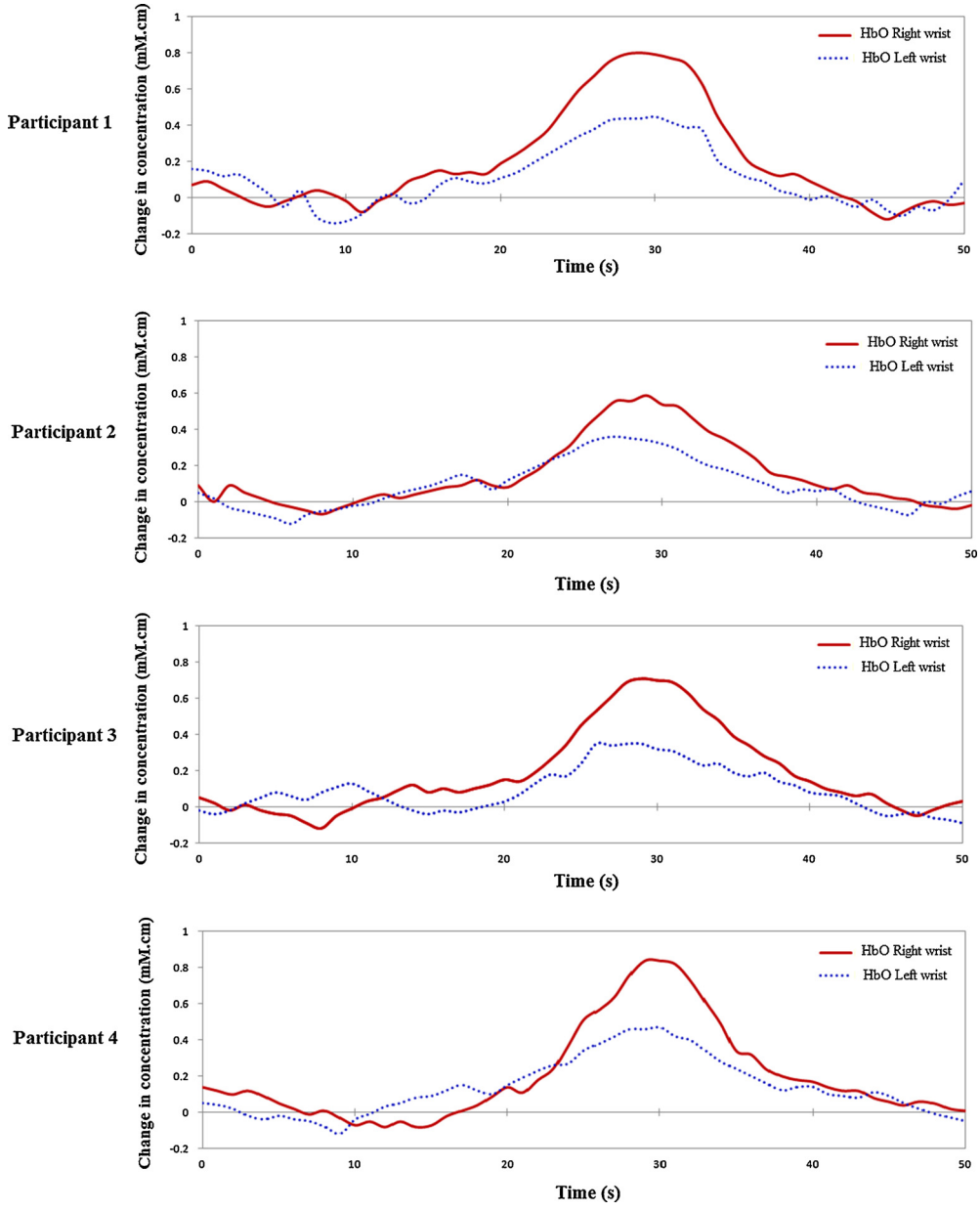

Fig. 2. Average ΔHbO responses: Average ΔHbO signals of participants 1, 2, 3 and 4 for the right- and left-wrist motor imagery.

achieved using SS 22–28 and SS 22–29 were improved to the level of those using SS within the total 10 s task period, the SS 22–27 was still observed to be the best performing feature among the group. The *p*-values for SS 22–27 versus SS 22–28, SS 22–29, SS 22–30 and SS 25–30 were 0.0180, 0.0029, 0.0007, and 6.0×10^{-5}, respectively. These results suggest that the 2–7 s time span within the total task period of 10 s is needed to classify, with high accuracies, the hemodynamic response corresponding to fNIRS signals.

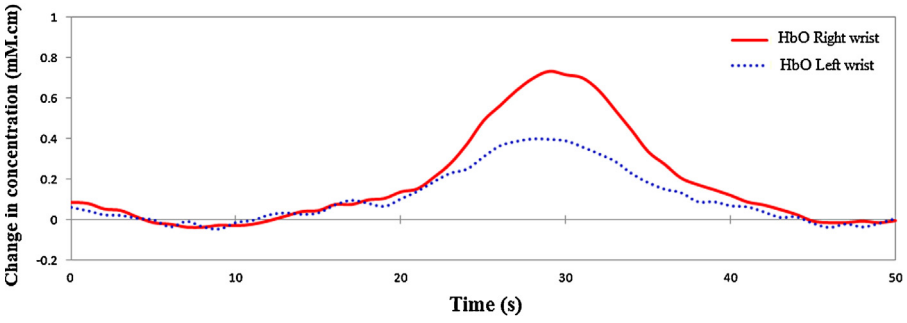

Fig. 3. Grand averages of ΔHbO response: Grand averages across all participants for the right-and left-wrist motor imagery.

Table 2
The classification accuracies with standard deviations according to SS for data acquired within 22–28 s, 22–29 s, 22–30 s and 25–30 s time windows.

Participant number	SS 22–28 [%]	SS 22–29 [%]	SS 22–30 [%]	SS 25–30 [%]
1	85.3 ± 6.51	84.2 ± 5.69	84.3 ± 6.05	80.4 ± 7.20
2	88.6 ± 7.47	85.6 ± 5.18	86.4 ± 5.81	83.1 ± 5.49
3	82.1 ± 4.95	78.1 ± 6.81	80.2 ± 6.54	73.2 ± 6.41
4	82.4 ± 6.79	82.9 ± 7.59	81.5 ± 8.10	80.4 ± 6.57
5	85.2 ± 6.11	84.5 ± 5.46	83.4 ± 5.24	80.5 ± 4.98
6	81.9 ± 8.09	82.2 ± 6.26	81.4 ± 6.36	79.6 ± 5.29
7	83.6 ± 7.51	84.6 ± 7.24	84.1 ± 4.77	81.5 ± 8.47
8	81.9 ± 5.81	82.2 ± 6.73	82.1 ± 7.51	79.4 ± 6.22
9	81.7 ± 6.33	84.6 ± 7.64	82.4 ± 5.88	81.8 ± 5.88
10	87.5 ± 5.16	83.4 ± 5.92	79.3 ± 6.49	83.7 ± 6.54
Average	84.02 ± 2.51	83.23 ± 2.12	82.51 ± 2.10	80.36 ± 2.88

The classification accuracies varied across the participants due to their individual differences [36], as can be seen in Tables 1 and 2; differences in head shape and scalp–cortex distance, for example, were potential sources of such variations. However, as Fig. 3 makes clear, the hemodynamic response patterns remained similar. A pertinent factor that should be noted is that, whereas BCI is primarily meant for totally locked-in individuals, all the participants in the present study were healthy. The hemodynamic responses of the people with amyotrophic lateral sclerosis, tetraplegia, and/or other motor impairments can differ from those of healthy individuals, which fact, as reported in [21], can result in relatively low classification accuracies. Another limitation of using fNIRS for BCI is that a real-time transmission of information is limited by the inherent delay in the hemodynamic response: the peak value occurs at approximately 5 s after the stimulus is applied [4]. Recently though, many studies have shown that such time delay can be reduced by detecting the fast optical response [9,13].

One of the limitations of our work is that we did not perform online classification; and certainly, for development of a real-time BCI using fNIRS, a single trial detection [28] and/or online classification [14] of fNIRS signals are required. Nonetheless, the real-time BCI using fNIRS remains a challenging task due especially to the inherent delays in the hemodynamic response. Another potential challenge is maintaining sufficient concentration during the motor imagery while making real-time results for imagery tasks.

5. Conclusions

This paper has presented results on fNIRS-based classification of the right- and left-wrist motor imageries using the LDA as the classifier. Participants were instructed to kinesthetically imagine the right- or left-wrist movements as indicated on a computer monitor. The right- and left-wrist motor imageries were classified using two distinct features, the signal mean (SM) and the signal slope (SS), during the whole 10 s task period as well as during different time windows within the task period. During the entire 10 s task period, the average classification accuracies were 73.35% and 83.0% using SM and SS, respectively. However, by reducing to 2–7 s time span within the task period, those accuracies were improved to 77.56% and 87.28%, respectively. Analyses of 6 different temporal windows show that the 2–7 s time span is the best temporal window size for classification.

Acknowledgment

This work was supported by the National Research Foundation of Korea funded by the Ministry of Education, Science and Technology, Korea (grant no. MEST-2012-R1A2A2A01046411).

References

[1] M. Aqil, K.-S. Hong, M.-Y. Jeong, S.S. Ge, Detection of event-related hemodynamic response to neuroactivation by dynamic modeling of brain activity, NeuroImage 63 (2012) 553–568.
[2] M. Aqil, K.-S. Hong, M.-Y. Jeong, S.S. Ge, Cortical brain imaging by adaptive filtering of NIRS signals, Neurosci. Lett. 514 (2012) 35–41.
[3] R. Beisteiner, P. Hollinger, G. Lindinger, W. Lang, A. Berthoz, Mental representations of movements: brain potentials associated with imagination of hand movements, Electroencephalogr. Clin. Neurophysiol. 96 (1995) 183–193.
[4] D.A. Benaron, S.R. Hintz, A. Villringer, D.A. Boas, A. Kleinschmidt, J. Frahm, C. Hirth, H. Obrig, J.C. van Houten, E.L. Kermit, W.F. Cheong, D.K. Stevenson, Noninvasive functional imaging of human brain using light, J. Cereb. Blood Flow Metab. 20 (2000) 469–477.
[5] S.M. Coyle, T.E. Ward, C.M. Markham, G. McDarby, On the suitability of near-infrared (NIR) systems for next generation brain–computer interfaces, Physiol. Meas. 25 (2004) 815–822.
[6] S.M. Coyle, T.E. Ward, C.M. Markham, Brain–computer interface using a simplified functional near-infrared spectroscopy system, J. Neural Eng. 4 (2007) 219–226.
[7] B. Frederick, L.D. Nickerson, Y. Tong, Physiological denoising of BOLD fMRI data using regressor interpolation at progressive time delays (RIPTiDe) processing of concurrent fMRI and near-infrared spectroscopy (NIRS), NeuroImage 60 (2012) 1913–1923.
[8] L. Gagnon, M.A. Yucel, M. Dehaes, R.J. Cooper, K.L. Perdue, J. Selb, T.J. Huppert, R.D. Hoge, D.A. Boas, Quantification of the cortical contribution to the NIRS signal over the motor cortex using concurrent NIRS-fMRI measurements, NeuroImage 59 (2012) 3933–3940.
[9] G. Gratton, C.R. Brumback, B.A. Gordon, M.A. Pearson, K.A. Low, M. Fabiani, Effects of measurement method, wavelength, and source–detector distance on the fast optical signal, NeuroImage 32 (2006) 1576–1590.
[10] L.R. Hochberg, D. Bacher, B. Jarosiewicz, N.Y. Masse, J.D. Simeral, J. Vogel, S. Haddadin, J. Liu, S.S. Cash, P. van der Smagt, J.P. Donoghue, Reach and grasp by people with tetraplegia using a neurally controlled robotic arm, Nature 485 (2012) 372–375.
[11] Y. Hoshi, Functional near-infrared spectroscopy: current status and future prospects, J. Biomed. Opt. 12 (2007) 062106.
[12] X.-S. Hu, K.-S. Hong, S.S. Ge, M.-Y. Jeong, Kalman estimator- and general linear model-based on-line brain activation mapping by near-infrared spectroscopy, Biomed. Eng. Online 9 (2010) 1–15.
[13] X.-S. Hu, K.-S. Hong, S.S. Ge, Recognition of stimulus-evoked neuronal optical response by identifying chaos levels of near-infrared spectroscopy time series, Neurosci. Lett. 504 (2011) 115–120.
[14] X.-S. Hu, K.-S. Hong, S.S. Ge, fNIRS-based online deception decoding, J. Neural Eng. 9 (2012) 026012.
[15] X.-S. Hu, K.-S. Hong, S.S. Ge, Reduction of trial-to-trial variations in functional near-infrared spectroscopy signals by accounting for resting-state functional connectivity, J. Biomed. Opt. 18 (2013) 017003.
[16] F.F. Jobsis, Noninvasive, infrared monitoring of cerebral and myocardial oxygen sufficiency and circulatory parameters, Science 198 (1977) 1264–1267.
[17] M.A. Kamran, K.-S. Hong, Linear parameter-varying model and adaptive filtering technique for detecting neuronal activities: an fNIRS study, J. Neural Eng. 10 (2013) 056002.
[18] F. Lotte, M. Congedo, A. Lecuyer, F. Lamarche, B. Arnaldi, A review of classification algorithms for EEG-based brain–computer interfaces, J. Neural Eng. 4 (2007) R1–R13.
[19] P.W. McCormick, M. Stewart, G. Lewis, M. Dujovny, J.I. Ausman, Intracerebral penetration of infrared light: technical note, J. Neurosurg. 76 (1992) 315–318.
[20] S. Moghimi, A. Khushki, S.D. Power, A.M. Guerguerian, T. Chau, Automatic detection of a prefrontal cortical response to emotionally rated music using multi-channel near-infrared spectroscopy, J. Neural Eng. 9 (2012) 026022.
[21] M. Naito, Y. Michioka, K. Ozawa, Y. Ito, M. Kiguchi, T. Kanazaw, A communication means for totally locked-in ALS patients based on changes in cerebral blood volume measured with near-infrared light, IEICE Trans. Inform. Syst. 90 (2007) 1028–1037.

[22] E. Okada, M. Firbank, M. Schweiger, S.R. Arridge, M. Cope, D.T. Delpy, Theortical and experimental investigation of near-infrared light propagation in a model of the adult head, Appl. Opt. 36 (1997) 21–31.
[23] G. Pfurtscheller, C. Neuper, A. Schlogl, K. Lugger, Separability of EEG signals recorded during right and left motor imagery using adaptive autoregressive parameters, IEEE Trans. Rehabil. Eng. 6 (1998) 316–325.
[24] G. Pfurtscheller, C. Neuper, C. Guger, W. Harkam, H. Ramoser, A. Schlogl, B. Obermaier, M. Pregenzer, Current trends in Graz brain–computer interface (BCI) research, IEEE Trans. Rehabil. Eng. 8 (2000) 216–219.
[25] C.A. Porro, M.P. Francescato, V. Cettolo, M.E. Diamond, P. Baraldi, C. Zuiani, M. Bazzocchi, P.E. di Prampero, Primary motor and sensory cortex activation during motor performance and motor imagery: a functional magnetic resonance imaging study, J. Neurosci. 16 (1996) 7688–7698.
[26] S.D. Power, A. Khushki, T. Chau, Towards a system-paced near-infrared spectroscopy brain–computer interface: differentiating prefrontal activity due to mental arithmetic and mental singing from the no-control state, J. Neural Eng. 8 (2011) 066004.
[27] S.D. Power, A. Khushki, T. Chau, Automatic single trial discrimination of mental arithmetic, mental singing and the no-control state from the prefrontal activity: towards a three-state NIRS-BCI, BMC Res. Notes 5 (2012) 141.
[28] S.D. Power, A. Kushki, T. Chau, Intersession consistency of single-trial classification of the prefrontal response to mental arithmetic and the no-control state by NIRS, PLoS ONE 7 (2012) e37791.
[29] M. Salvaris, F. Sepulveda, Classification effects of real and imaginary movement selective attention tasks on a P300-based brain–computer interface, J. Neural Eng. 7 (2010) 056004.
[30] H. Santosa, M.J. Hong, S.-P. Kim, K.-S. Hong, Noise reduction in functional near-infrared spectroscopy signals by independent component analysis, Rev. Sci. Instrum. 84 (2013) 073106.
[31] R. Sitaram, H. Zhang, C. Guan, M. Thulasidas, Y. Hoshi, A. Ishikawa, K. Shimizu, N. Birbaumer, Temporal classification of multichannel near-infrared spectroscopy signals of motor imagery for developing a brain–computer interface, NeuroImage 34 (2007) 1416–1427.
[32] D. Szollosi, L.D. Denes, F. Firtha, Z. Kovacs, A. Fekete, Comparison of six multiclass classifiers by the use of different classification performance indicators, J. Chemomtr. 26 (2012) 76–84.
[33] A. Vuckovic, F. Sepulveda, A two-staged four-class BCI based on imaginary movements of the left and right wrist, Med. Eng. Phys. 34 (2012) 964–971.
[34] J.R. Wolpaw, N. Birbaumer, D.J. McFarland, G. Pfurtscheller, T.M. Vaughan, Brain–computer interfaces for communication and control, Clin. Neurophysiol. 113 (2002) 767–791.
[35] G.R. Wylie, H.L. Graber, G.T. Voelbel, A.D. Kohl, J. DeLuca, Y.L. Pei, Y. Xu, R.L. Barbour, Using co-variations in the Hb signal to detect visual activation: a near-infrared spectroscopic imaging study, NeuroImage 47 (2009) 473–481.
[36] T. Yarkoni, T.S. Braver, Cognitive neuroscience approaches to individual differences in working memory and executive control: conceptual and methodological issues, in: A. Gruszka, G. Matthews, B. Szymuyra (Eds.), Handbook of Individual Differences in Cognition: Attention, Memory and Executive Control, Springer, New York, 2010, pp. 87–107.